Further evidence of the increase in energy spacing in the dot channel is the decrease in valley current (I_v) when more electrons are charged into the floating gate, as shown in Fig. 4, where the valley positions are indicated for three different charge densities on the floating dot gate. Since $I_v \propto \exp(-\Delta E/2kT)$, the reduction in the valley current implies the increase in energy level separation.

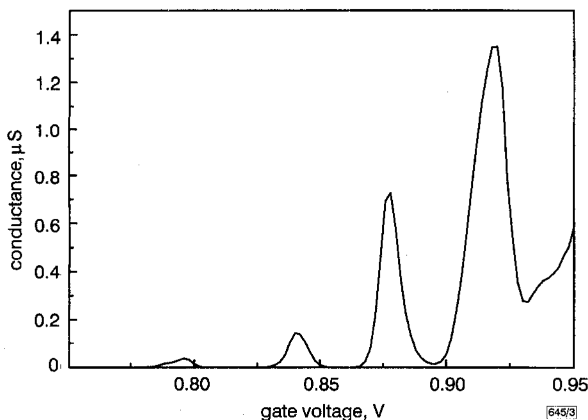

Fig. 3 *Conductance oscillations of stacked QDT taken at 4.2K after floating gate was charged with electrons*

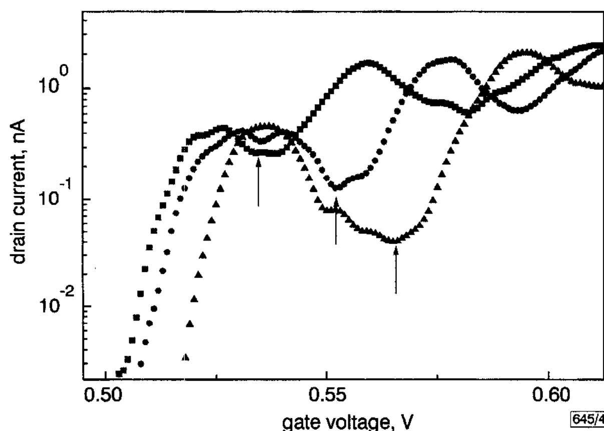

Fig. 4 *Drain current against gate voltage, showing decrease of valley current with charging of floating gate*

Charging carried out by applying 10ms, 13V pulses to control gate
■ 5 pulses
● 10 pulses
▲ 15 pulses
Source drain bias: 1.2mV

In this case, incremental charging was performed by applying a series of voltage pulses of 13V to the control gate. The increase in energy level separation was estimated to be 1.5 and 2.3meV after each incremental charging. Both observations indicate that charging of the floating gate can enhance the charge confinement in the Si dot. This process is also reversible: after the electrons were removed from the floating gate, the transistor's I-V characteristics returned to its original behaviour before charging.

Such an effect can be attributed to the Coulomb interaction between the electrons in the floating gate and those in the Si channel dot. Before the floating gate is charged, the electrons in the channel dot can distribute throughout the vertical direction of the thin silicon film, owing to volume inversion formed near the threshold [7]. However, when the negative charges are stored in the floating gate, because of the Coulomb repulsion, the channel electrons are depleted away from the interface between the silicon channel and the tunnel oxide. That is, the electron distribution in the channel dot was compressed, leading to a smaller effective quantum dot. In this case, the Coulomb charging energy increases as a result of the effective size reduction of the quantum dot.

In conclusion, we have demonstrated a quantum dot transistor with a polysilicon dot floating gate stacked on top of an Si dot channel. By charging the floating dot, not only can the threshold voltage of the transistor be shifted, but also the conductance oscillations in the quantum dot channel can be greatly enhanced. Such an enhancement is attributed to the reduction of the effective quantum dot size, which leads to an increase in energy level separation.

Acknowledgments: This work was partially supported by ONR, DARPA and ARO.

© IEE 1998
25 March 1998
Electronics Letters Online No: 19980717

L.J. Guo and S.Y. Chou (*NanoStructure Laboratory, Department of Electrical Engineering, Princeton University, NJ 08544, USA*)

References

1 TAKAHASHI, Y., NAGASE, M., NAMATSU, H., KURIHARA, K., IWDATE, K., NAKAJIMA, Y., HORIGUCHI, S., MURASE, K., and TABE, M.: 'Conductance oscillations of a Si single electron transistor at room temperature'. IEDM Tech. Dig., 1994, pp. 938–940

2 YANO, K., ISHII, T., HASHIMOTO, T., KOBAYASHI, T., MURAI, F., and SEKI, K.: 'A room temperature single-electron memory device using fine-grain polycrystalline silicon'. IEDM Tech. Dig., 1993, pp. 541–544

3 GUO, L.J., LEOBANDUNG, E., and CHOU, S.Y.: 'A silicon single-electron transistor memory operating at room temperature', *Science*, 1997, **275**, (5300), pp. 649–651

4 LEOBANDUNG, E., GUO, L.J., and CHOU, S.Y.: 'Electron and hole silicon quantum dot transistors operating above 100 K', *J. Vac. Sci. Technol. B*, 1995, **13**, (6), pp. 2865–2868

5 GRABET, H., and DEVORET, M.H.: 'Single charge tunneling: Coulomb blockade phenomena in nanostructures' (Plenum, New York, 1992)

6 BEENAKKER, C.W.J.: 'Theory of Coulomb-blockade oscillations in the conductance of a quantum dot', *Phys. Rev. B*, 1991, **44**, pp. 1646–1656

7 BALESTRA, F., CRISTOLOVEANU, S., BENACHIR, M., BRINI, J., and ELEWA, T.: 'Double-gate silicon-on-insulator transistor with volume inversion: a new device with greatly enhanced performance', *IEEE Electron Device Lett.*, 1987, **EDL-8**, (9), pp. 410–412

Surface recombination related frequency dispersion of current gain in AlGaAs/GaAs HBTs

B. Ihn, J. Lee, T.M. Roh, Y.S. Kim and B. Kim

The dispersion effect of current gain related to surface recombination in AlGaAs/GaAs HBTs has been studied. For an HBT with an emitter area of 3 × 20µm², the surface recombination current-to-total base current ratio is ~ 0.47 at < 100MHz, and the ratio is decreased to zero at frequencies between 100MHz and 3GHz, clearly indicating that the current gain is dispersive.

Introduction: AlGaAs/GaAs heterojunction bipolar transistors (HBTs) are applicable for high speed digital and microwave circuits. In order to obtain the required high f_t and f_{max}, emitter size reduction is essential. As the emitter size decreases, surface recombination at the emitter periphery increases and current gain also decreases. Many studies have attempted to characterise the base surface recombination current effect [1, 2]. However, few reports are available on the frequency-dependence of this current component. In fact, the frequency dispersion of output resistance (R_{ds}) and transconductance (g_m) of GaAs MESFETs have been investigated by many authors, and these phenomena are explained by surface-states [3, 4]. In this work, we report that HBTs also have current gain dispersion which is related to surface recombination.

Device structures and measurements: The MOCVD-grown epi-layer structure has a 700Å thick, 30% Al mole fraction emitter layer and 1000Å thick carbon-doped base layer. The emitter, base, and collector dopant concentrations are 2×10^{17}, 2×10^{19}, and 2×10^{16}cm^{-3}, respectively. Several different sized HBTs are fabricated by a conventional MESA-type self-aligned base metal HBT process without adopting any surface passivation. Devices with four different emitter sizes were measured; 4 × 30, 4 × 10, 3 × 30, and 3

× 20μm², respectively. All the measured devices were close together on the same wafer. The perimeter-to-area ratio (p/A) was 0.57, 0.7, 0.73, and 0.77μm⁻¹, respectively. The RF characteristics of the HBTs were measured with a Tektronix 370 programmable curve tracer and HP 8510B network analyser in the frequency range from 45MHz to 18GHz.

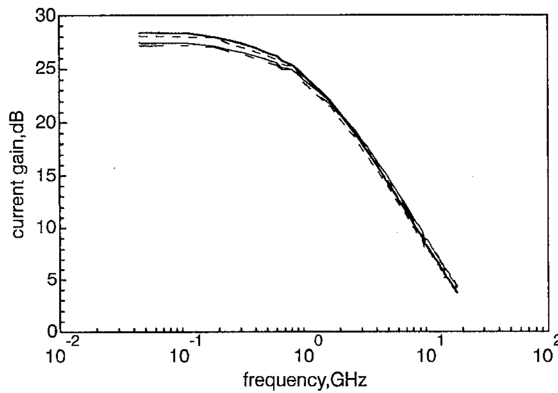

Fig. 1 *Current gain against operational frequency of fabricated HBTs with various emitter sizes*

$J_c = 5 \times 10^3 A/cm^2$
——— 4 × 30μm²
– – – – 4 × 10μm²
——— 3 × 30μm²
— — — 3 × 20μm²

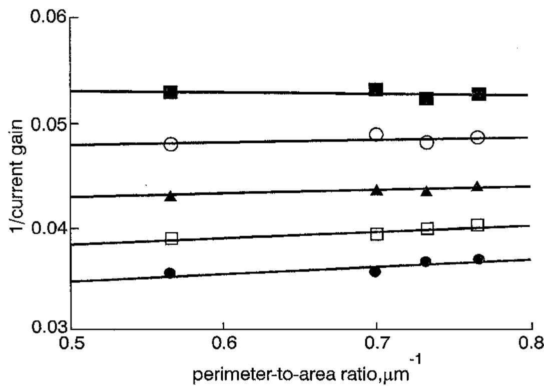

Fig. 2 *Current gain against perimeter-to-area ratio (p/A) for four different size HBTs at different frequencies*

$J_c = 5 \times 10^3 A/cm^2$
—●— 45MHz
—□— 667MHz
—▲— 1.4GHz
—○— 2.0GHz
—■— 2.7GHz

Results and discussion: Fig. 1 shows the current gains of different emitter size HBTs at the same collector current density. It shows that the values of h_{fe} are different at low frequencies but tended to the same value at high frequencies. If the measurement frequency is higher than the characteristic frequency (f_o) of the surface-states, the surface-state occupancy will be unable to follow the signal [3]. Therefore, the surface recombination current component will vanish and h_{fe}s become identical. The frequency dependent surface recombination current component can be extracted from the relationship between the current gain and perimeter-to-area (p/A) ratio expressed as eqns. 1 and 2.

$$\left.\frac{1}{h_{fe}}\right|_{\text{at fixed frequency}} = \frac{\Delta i_b^i + \Delta i_b^s}{\Delta i_c}$$

$$= \frac{1}{h_{fe}^i} + \frac{\Delta j_b^s}{\Delta j_c} \times \frac{p}{A} \quad (f < f_o) \quad (1)$$

$$= \frac{1}{h_{fe}^i} \quad (f > f_o) \quad (2)$$

where Δi_b^i, Δi_b^s, and Δi_c are the changes in intrinsic base current, base surface recombination current, and collector current, respectively. Δ_{jb}^s and Δj_c are the changes in base recombination current density per unit emitter periphery and collector current density per unit emitter area, respectively. h_{fe}^i is the intrinsic current gain without surface recombination. The values of h_{fe}^i and $\Delta i_b^s/\Delta i_b$ are obtained from the intercept point and slope of a least-squares fit of the h_{fe}^{-1} against p/A data. Fig. 2 depicts this relationship at five different frequencies. This Figure shows that as frequency

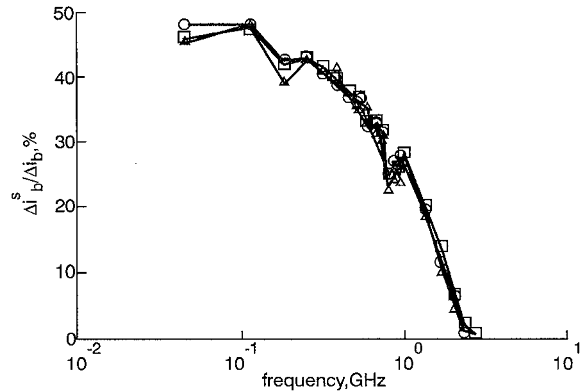

Fig. 3 *Total base current-to-base surface recombination current ratio ($\Delta i_b^s/\Delta i_b$) against frequency at various collector current densities*

$A_E = 3 \times 20\ \mu m^2$
—▽— $J_c = 5 \times 10^3 A/cm^2$
—□— $J_c = 8 \times 10^3 A/cm^2$
—○— $J_c = 1 \times 10^4 A/cm^2$

increases, the slope reduces. At ~ 2.7GHz the slope is zero, indicating that base surface recombination current is zero. Fig. 3 shows the surface recombination current component at various frequencies. The surface recombination current component Δi_b^s is ~ 47% of total base current at < 100MHz and decreases as frequency increases, finally vanishing at ~ 3GHz. Fig. 4 shows interesting data in which h_{fe}, h_{fe}^i, and h_{fe}^s are compared. Here h_{fe}^s is the current gain under the condition that the recombination responds very fast. At low frequencies, h_{fe} follows h_{fe}^s because of the surface recombination, but as frequency increases, the surface-states cannot respond and the curve follows h_{fe}^i. The frequencies of the dispersion region in HBTs are much higher than those of GaAs MESFETs (10Hz ~ 1MHz) [3, 4] in spite of the similar mechanism. The surface recombination velocity increases as the doping density increases [5]. The base doping in HBTs is about two orders of magnitude higher than the channel doping in GaAs MESFETs. This means that the surface state lifetime of HBTS is a lot shorter than that of MESFETs.

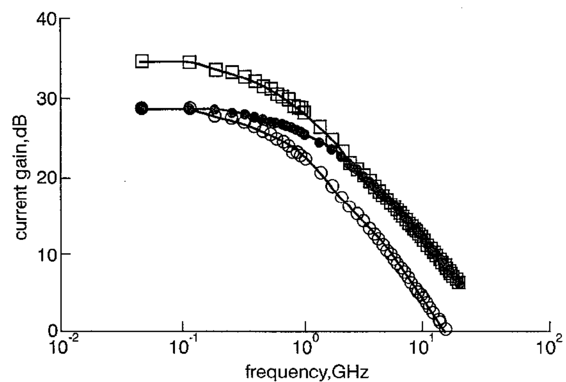

Fig. 4 *h_{fe}, h_{fe}^i and h_{fe}^s against frequency*

$J_c = 1 \times 10^4 A/cm^2$
—○— h_{fe}^s (intrinsic current gain without surface recombination)
—□— h_{fe}^i (current gain with fast surface-states)
—●— h_{fe}

Conclusions: In conclusion, we have studied the surface recombination related frequency dispersion of current gain in AlGaAs/GaAs HBTs for the first time. $\Delta i_b^s/\Delta i_b$ is ~ 47% at < 100MHz (A_E = 3 × 20μm²), and the transition frequency is between 100MHz and 3GHz. These results indicate that more exact large-signal modelling including the dispersion effect is required for accurate circuit simulation, especially for mobile communication systems whose operation frequencies coincide.

Acknowledgment: This work has been partially supported by the Korea Agency for Defense Development and Korea Telecommunication.

© IEE 1998
4 March 1998
Electronics Letters Online No: 19980701

B. Ihn (*Photonics Laboratory, Samsung Advanced Institute of Technology, PO Box 111, Suwon 440-600, Korea*)

ibu@saitgw.sait.samsung.co.kr

J. Lee (*R&D Lab.2, Mobile Telecommunications Terminal Division, Hyundai Electronics Industries Co., Ltd., PO Box 1010, Ichon-shi, Kyounggy-do, 467-701, Korea*)

T.M. Roh (*Wireless Terminals Division, Samsung Electronics, 94-1, Imsudong, Kumi-shi, Kyungbuk, Korea*)

Y.S. Kim and B. Kim (*Department of Electrical and Electronic Engineering and Microwave Application Research Center, Pohang University of Science and Technology, San-31 Hyoja-song, Nam-ku, Pohang, Kyungbuk, 790-784, Korea*)

References

1 HAYAMA, N., and HONJO, K.: 'Emitter size effect on current gain in fully self-aligned AlGaAs/GaAs HBT's with AlGaAs surface passivation layer', *IEEE Electron Device Lett.*, 1990, **11**, pp. 388–390

2 LIU, W., and HARRIS, J.S.: 'Diode ideality factor for surface recombination current in AlGaAs/GaAs heterojunction bipolar transistors', *IEEE Trans. Electron Devices*, 1992, **ED-39**, pp. 2726–2732

3 LADBROOKE, P.H., and BLIGHT, S.R.: 'Low-field low-frequency dispersion of transconductance in GaAs MESFET's with implications for other rate-dependent anomalies', *IEEE Trans. Electron Devices*, 1988, **ED-35**, pp. 257–267

4 GOLIO, J.M., MILLER, M.C., MARACAS, G.N., and JOHNSON, D.A.: 'Frequency-dependent electrical characteristics of GaAs MESFET's', *IEEE Trans. Electron Devices*, 1990, **ED-37**, pp. 1217–1227

5 ASPNES, D.E.: 'Recombination at semiconductor surfaces and interfaces', *Surface Sci.*, 1983, **132**, pp. 406–421

High voltage pulse tuning of strontium titanate TM_{010} disk resonator

O.G. Vendik, A.N. Rogatchev and L.T. Ter-Martirosyan

The microwave response of a parallel plate dielectric resonator, made of bulk single crystal $SrTiO_3$ coated with thin $YBa_2Cu_3O_{7-x}$ film, is investigated when a pulse voltage is applied. Pulses of ~1kV amplitude, and 1ms leading and 3μs trailing fronts, were used. No relaxation process in the material of the disk resonator has been observed.

Introduction: The disk resonator made from single crystal $SrTiO_3$ (STO), plated with $YBa_2Cu_3O_{7-x}$ (YBCO) film electrodes [1] is of interest for many applications because it can be used as a basis for tunable resonators or filters [2, 3]. It was observed that under the bias voltage the quality factor of the resonator decreases sharply, and accordingly tanδ of STO was remarkably increased under the bias voltage [1]. In this Letter we demonstrate the tunability of an STO resonator under short, high voltage pulses and make an estimation of the influence of the space charge in the STO on the tunability and tanδ of the material. The goal of the experiment is to investigate the special features of tunability of the STO resonator by voltage pulses as compared with tunability under DC voltage. It is known that an imperfect ferroelectric crystal contains regions with residual ferroelectric polarisation [4] and lattice defects forming dip traps for charge carriers [5, 6]. Besides this, the charges localised in depletion layers near electrodes or immediately injected from the electrodes under a high electric field should be taken into account [7]. The processes connected with the space charge in the STO sample are characterised by a large spectrum of different time constants in the range from a few μs to a few min [5]. In order to distinguish the time relaxation processes in the disk resonator, we used pulsed bias voltage with an amplitude near 1000 V and different durations of the pulse fronts.

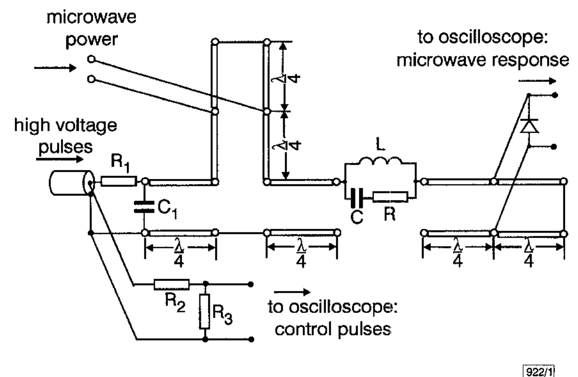

Fig. 1 *Equivalent circuit of experimental setup*

Resistance and capacitance in separating network are R_1 = 1.2 × 10³ Ω, C_1 = 100pF

Experimental setup: The base of the experimental setup was the same as that described in [1] with some new network components which were added to provide operation under high voltage pulses. The equivalent circuit of the experimental setup is shown in Fig. 1. The device under test was a single crystal STO disk of 10mm diameter and 0.6mm thickness. YBCO film electrodes, 300nm thick, were sputtered using laser ablation onto both sides of the disk. The transition temperature of the YBCO films was 90–91K. The experimental setup with the disk resonator was immersed in liquid nitrogen. Measurements were carried out at T = 78 ± 0.5K. For measurements of the microwave (MW) performance, the resonator was included in the central conductor of a coaxial line. The mode TM_{010} was excited in the resonator. The diameter of the central conductor of the line was d = 10mm, and the wave impedance of the line was Z_0 = 15Ω. A set of quarter-wavelength transformers provides impedance matching for the coaxial line with a standard coaxial cable. The MW equipment was protected against high voltage shock by short-circuited λ/4 transmission line sections. The high voltage pulses were formed by a thyristor circuit, which provides a leading front duration of ~1ms and a trailing front duration of ~3μs. The DC capacitance of the disk resonator is 2300pF. The DC current flowing through the STO disk under the DC voltage 1000V was < 0.1μA. The bias pulse voltage amplitude was 680V.

Theory: In order to describe the phenomenon investigated, a simple model has been developed. We assumed the resonant frequency and the quality factor of the resonator to be described by the following functions:

$$\omega(U) = \omega_0\sqrt{1 + \left(\frac{U}{U_0}\right)^2}$$
$$Q(U) = Q_o\left[1 + A\left(\frac{U}{U_0}\right)^2\right]^{-1} \quad (1)$$

where U_0 and A are parameters of the model.

The resonant frequency of the STO disk resonator is determined by the field dependence of the STO dielectric constant. The model used is in reasonable agreement with the rigorous model of the dielectric response of the incipient ferroelectric [8]. The dependence of Q-factor on voltage is in agreement with the dependence of STO tanδ on the field in the case of loss contributed by a residual ferroelectric polarisation [9].